Eur. Phys. J. C (2023) 83:1038
https://doi.org/10.1140/epjc/s10052-023-12207-1

THE EUROPEAN PHYSICAL JOURNAL C

Regular Article - Theoretical Physics

New mass limit of a strange star admitting a colour flavor locked equation of state

K. B. Goswami[1,a], **A. Saha**[1,2,b], **P. K. Chattopadhyay**[1,c], **S. Karmakar**[3,d]

[1] Department of Physics, Coochbehar Panchanan Barma University, Vivekananda Street, Coochbehar, West Bengal 736101, India
[2] Department of Physics, Alipurduar College, Alipurduar, West Bengal 736122, India
[3] Department of Physics, University of North Bengal, Raja Rammohunpur, P.O.-N.B.U., Darjeeling, West Bengal 734013, India

Received: 22 May 2023 / Accepted: 30 October 2023 / Published online: 15 November 2023

Abstract A class of strange stars is analysed in the present article in hydrostatic equilibrium, whose state is defined by a CFL phase equation of state. We have compared our results with those obtained from the MIT equation of state for strange quark matter, which is regarded as free particles. We have noted that if we consider quarks to form a cooper pair and if their description is made by the CFL equation of state, the maximum mass of strange star reaches a value as high as 3.61 $M_{\odot}$. This value is well above the value of 2.03 $M_{\odot}$ obtained by using the MIT bag equation of state for massless free quarks. Both the maximum masses are determined by solving the TOV equation for different values of the strange quark mass m_s. Thus, the inclusion of the possibility of quark pair formation in the theory permits us to accommodate a wider class of compact objects such as PSR J1614-2230, PSR J0740+6620, PSR J0952-0607 etc. and the mass of the companion star in the GW190814 event in our model. The consideration of such a high value of mass is hardly theoretically obtainable from normal strange star models in general relativity even with a fast rotation effect. The object PSR J0952-0607 is found to be the fastest and heaviest pulsar in the disk of Milky Way Galaxy, having a mass of 2.35 $M_{\odot}$, which may be predicted in our model, as observational evidence supports the existence of strange quark matter in its composition.

1 Introduction

The objective that strange quark matter (henceforth SQM) may be the true ground state of quantum chromodynamics (henceforth QCD) was first suggested by Witten [1] in 1984. The basic concept is that in the case of SQM, the energy associated with each baryon might be lower than that of the energy per baryon of the most stable nucleus, ^{56}Fe, making SQM more stable. According to the asymptotic behaviour of QCD, nucleons are split into the form of quarks, and these weakly interacting deconfined quarks constitute a gas. Theories used for the description of hadron to quark phase transition are phenomenological. One such model is the bag model [2], which contributes to the suitable description of the bulk quark matter and also its confinement in a region of space called a "bag", containing hadronic fields. The bag has a constant, positive potential energy per unit volume. This constant is known as vacuum energy B, also termed the bag constant. In the context of the MIT bag model, Farhi and Jaffe [3] studied the properties of SQM extensively considering different choices of B and the mass of a strange quark (m_s). They established a stability window for stable SQM in the ($m_s - B$) plane. In the context of general relativity (henceforth GR), a number of authors have used the MIT bag equation of state (henceforth EoS) to qualitatively study compact stars composed of quark matter [4–8]. If the hypothesis of strange matter is correct, a possibility of a new class of compact object made entirely of SQM, called the "Strange Star", should exist. The possible existence of strange stars has been studied by many researchers [9,10], and it has been confirmed theoretically that stable strange star configurations are possible. These stars are much smaller in size than normal neutron stars because they are self-bound due to strong interaction and fundamentally different in comparison to the gravitationally bound neutron stars [9,10]. Recently, a large

[a] e-mail: koushik.kbg@gmail.com
[b] e-mail: anirban.astro9@gmail.com
[c] e-mail: pkc_76@rediffmail.com (corresponding author)
[d] e-mail: skarma78@rediffmail.com

group of researchers have studied compact stars extensively composed of SQM [11–15].

There has been a vast theoretical progress in the understanding of SQM. It is well established that in the presence of weak attractive interactions arbitrary in nature, degenerate Fermi systems are unstable. Such a problem of instability is solved by considering the formation of Cooper pairs in the Bose condensate form, leading to superconductivity for charged fermions. Similarly, at low temperature and sufficiently high baryon number density, the presence of attractive interactions between quarks will lead to the formation of quark Cooper pairs, which are responsible for colour superconductivity. It is now well admitted that colour flavor locked (henceforth CFL) strange matter is the true ground state of strong interaction [16]. At temperatures much lower than quark chemical potentials ($T \ll \mu$), several spontaneous symmetry breaking phases occur. In nature, this only happens in the interior of compact objects where matter density exceeds nuclear matter density. The time span of such objects is high enough to attain a state of equilibrium through weak interactions and to reduce the temperature below the chemical potential of quarks. It is expected that at low temperatures and ultrahigh densities, hadrons may break into a degenerate soup of quarks, forming Cooper pairs near the Fermi surface that exhibit colour superconductivity. Quark Cooper pair formation was noted long before the development of any consistent theory of strong interaction [17,18]. The study of quark Cooper pair formation originated after the pioneering works of Barrois [19,20] and Frautschi [21]. Making use of the CFL EoS, Bogadi et al. [22] investigated the surface tension of strange quark stars in hydrostatic equilibrium. In their work, they employed the Finch-Skeaansatz and thereby studied the mass–radius profile of such stars. They found that by properly choosing the strange quark mass (m_s) and the QCD gap energy (Δ_G), the mass and radius of a few strange star candidates may be predicted that are closest to the observational data. Thirukkanesh et al. [23] obtained a general solution of the Einstein field equation for a colour flavor locked EoS. They showed that by switching off a parameter, the CFL phase EoS reduces to a linear form that mimics the MIT bag model EoS. Reference [24] discussed further development in this field.

Most of the studies of SQM in both the normal and CFL phases initiated the concept of vacuum energy based on the idea of a phenomenological bag constant, B. However, due to the high densities in the vicinity of the core of the compact stars/ strange stars, it is more practical to demand that the bag constant should be density dependent [25]. Several works have been done on density-dependent bag constants [26–32]. Thermodynamics and the EoS of the SQM are different if one considers the density-dependent B from those with constant B.

In the case of a compact object, with exceedingly high matter density, it is expected that the internal pressure consists of two parts [33], namely, (i) radial pressure (p_r) and (ii) transverse pressure (p_t). The existence of type 3A superfluid or a solid core interior to a compact object may explain the presence of anisotropic pressure in the high density regime [34]. As nucleons are fermions, they obey the Pauli exclusion principle and therefore cannot occupy the same energy state. However, at low temperature, nucleons may form cooper pairs [35], which are virtually bosons and behave collectively. Thus, at very low temperature, nucleons behave collectively on a large scale and form nucleon condensates. This nucleon condensate is analogous to He-3 and flows without viscosity. The high-pressure environment inside a compact object, especially in a Neutron Star or Strange Star, increases the critical temperature of cooper pair formation, making nuclear superfluidity to exist even at a temperature of billion degrees. Anisotropy may also arise from pion condensation [36] and different types of phase transitions [37].

Our objective here is to study the strange star with a density-dependent bag constant model and compare it with an exactly solvable Vaidya–Tikekar model [38,39]. In the Vaidya–Tikekar model, the g_{rr} metric component extensively depends on the spheroidal parameter λ and curvature parameter R. This implies that the physical 3-space associated with the star possesses the geometry of a 3-spheroid immersed in a four-dimensional Euclidean flat space. Using V–T ansatz, Sharma et al. [40] have shown that by fine tuning λ or bag constant B, the observed mass radius of a wider range of compact objects may be predicted from theoretical model. Goswami et al. [41] recently obtained the radius and maximum mass of strange stars whose interior may be described by the MIT bag EoS in the V–T model. They also showed that a correlation between the spheroidal parameter λ and bag constant B exists so that the observed mass and radius of some compact objects may be predicted from their model. The prime goal of the present article is to conduct a comparative study between quark matter in the CFL phase EoS and MIT bag EoS and their astrophysical implications. The thermodynamically obtained pressure density relation has been related to that obtained by solving the Einstein Field equations for metric ansatz of Vaidya and Tikekar.

The paper is arranged in the following sequences: in Sect. 2, we have given a brief outline of the thermodynamic properties of SQM and the EoS in the MIT bag model. Section 3 consists of a density-dependent bag model as proposed by previous authors, while the origin of the density-dependent bag constant (B) has been discussed on a thermodynamic standpoint in Sect. 4. The EoS of quarks in the CFL phase is outlined in Sect. 5. In Sect. 6, the solutions of the Einstein Field equations are presented for Vaidya–Tikekar ansatz. Hence, the mathematical expressions of energy density and pressure have been obtained. Next, we used the

thermodynamically obtained EoS for both the CFL and MIT bag EoS and incorporated them into the mathematical model stated in Sect. 7. A comparison of both EoSs has been made, which is also discussed in this section. In Sect. 8, we have shown the mass–radius relation of strange stars in the CFL and MIT bag EoS. The energy conditions are plotted in Sect. 9. The stability of the model has been studied in view of the Herrera cracking concept and the nature of the adiabatic index, which have been represented in Sects. 10 and 11. Finally, we make concluding remarks on our model by mentioning some of the striking features in Sect. 12.

2 General properties of SQM

SQM is composed of Fermi gas comprised of massless u and d quarks, massive strange (s) quarks of mass m_s and electrons. The chemical equilibrium between the particles is sustained through the weak interactions

$$d, s \leftrightarrow u + e + \overline{\nu}_e; \quad s + u \leftrightarrow u + d. \tag{1}$$

The properties of strange matter are determined by their thermodynamic potentials $\Omega_i (i = u, d, s, e^-)$, which are functions of chemical potentials μ_i as well as m_s and the strong interaction coupling constant α_c [3]. The weak interactions given by Eq. (1) imply that the chemical potentials μ_i should satisfy

$$\mu_d = \mu_s \equiv \mu; \quad \mu_u + \mu_e = \mu \tag{2}$$

and the charge neutrality condition requires

$$\frac{2}{3}n_u - \frac{1}{3}n_d - \frac{1}{3}n_s - n_e = 0, \tag{3}$$

where n_i is known as the number density of the ith type particle given by $n_i = -(\frac{\partial \Omega_i}{\partial \mu_i})$. Equations (2) and (3) imply that there is only one independent chemical potential denoted by μ. The pressure (p), energy density (ρ) and baryon number density (n) of the quark phase are evaluated from the following relations:

$$p = -\sum_i \Omega_i - B, \tag{4}$$

$$\rho = \sum_i (\Omega_i + \mu_i n_i) + B, \tag{5}$$

$$n = \frac{1}{3}(n_u + n_d + n_s). \tag{6}$$

To obtain the EoS, one has to eliminate μ from Eq. (4) and express ρ and n as a function of pressure p using Eqs. (5) and (6). Witten [1] considered $m_s \to 0$, $\alpha_c \to 0$ in the case of a neutron star and gave the EoS of the quark matter approximately as

$$p = \frac{1}{3}(\rho - 4B). \tag{7}$$

In Eq. (7), B is referred to as the bag constant. In the MIT bag model, the constituent quarks are assumed to be in a confined state inside a perturbative vacuum or 'bag'. The confinement occurs due to the presence of a net inward pressure B exerted by the surrounding nonperturbative vacuum. With an increase in the baryon number density n, the separation between these two vacua may disappear, and consequently, the bag constant, which is basically the net inward pressure, must vanish. Therefore, it is physically more realistic to consider B as a density-dependent quantity [25].

3 Density dependent bag constant

Originally, the bag constant was kept fixed as its free space value in the bag model. Since the deconfinement phase transition depends on both the temperature and the number density of baryons in the system, the bag constant may be temperature dependent [42] as well as density dependent [43–45]. The bag constant, which depends on the temperature, describes the scenario of heavy-ion collision in the high-energy regime of terrestrial laboratories, whereas the density-dependent bag constant describes cold compact stars. Prasad and Bhalerao [31] considered three forms of the density-dependent B published by three different groups:

1. They have fitted the results obtained by [43] to express B analytically as

$$B(n) = B(0) exp[-(a_1 x^2 + a_2 x)], \tag{8}$$

where n is the baryon number density and $x = \frac{n}{n_0}$ is the normalized number density of baryons. Where $n_0 = 0.17\ fm^{-3}$ represents the baryon number density of the ordinary nuclear matter, $a_1 = 0.0125657$, $a_2 = 0.29522$ and $B(0) = 114\ \text{MeV}/fm^3 = (172\ \text{MeV})^4$.
2. Burgio et al. [44] have presented B in terms of a parametric form given below:

$$B(n) = B_{as} + (B_0 - B_{as}) exp[-\beta_n x^2], \tag{9}$$

where $B_{as} = 38\ \text{MeV/fm}^3$, $B_0 = 200\ \text{MeV/fm}^3$, $\beta_n = 0.14$.
3. Aguirre [45] has calculated a density-dependent B to study SQM in the CFL phase, which is given by

$$B(n) = a + \sum_{i=1}^{5} b_i x^i, \ x \le 9;$$
$$B(n) = \beta_n exp[-\alpha_n (x - 9)], \ x > 9, \tag{10}$$

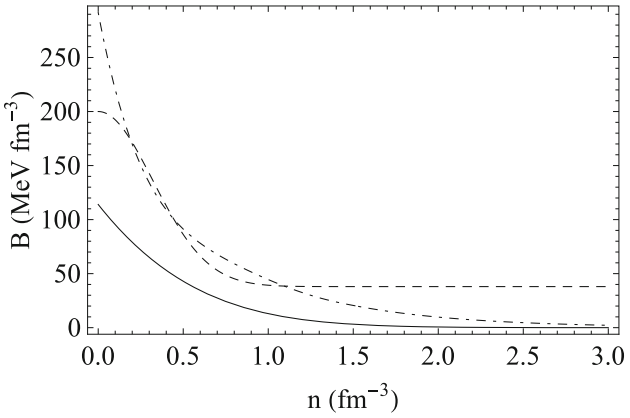

Fig. 1 Bag constant B vs baryon number density n for the three models. The solid line is for Liu et al. [43], the dot-dashed line is for Aguirre et al. [45] and the dashed line is for Burgio et al. [44]

where $a = 291.5906$, $b_1 = -142.25581$, $b_2 = 39.29997$, $b_3 = -6.04592$, $b_4 = 0.46817$, $b_5 = -0.01421$, $\alpha_n = 0.253470705$ and $\beta_n = 19.68764$.

The density dependent B given above is displayed in Fig. 1. The above three models give the value of B over a broad range of densities that exist in the strange star.

4 Thermodynamics with density dependent B

Here, we have followed a similar mechanism adopted by Zhu et al. [32]. First, we have derived from the general ensemble theory the expression for the energy and pressure of a system of particles when the particle masses are dependent on density. The partition function is given by

$$\Xi = \sum_{N_i,\alpha_c} e^{-\beta(E_{N_i,\alpha_c} - \sum_i \mu_i N_i)}, \tag{11}$$

where β is the reverse temperature, and N_i and μ_i represent the particle numbers and chemical potentials of the ith type particle, respectively. The microscopic energy $E_{N_i,\alpha} = f(V, m_i, N_i, \alpha_c)$, where V, m_i, N_i and α_c represent the volume of the system, particle masses, particle numbers and other quantum numbers, respectively. The pressure of such a system is defined as

$$\begin{aligned} p &= \frac{1}{\Xi} \sum_{N_i,\alpha_c} \left(-\frac{\partial E_{N_{i,\alpha_c}}}{\partial V} \right) e^{-\beta(E_{N_i,\alpha_c} - \sum_i \mu_i N_i)} \\ &= \frac{1}{\beta} \frac{\partial ln\Xi}{\partial V} = -\frac{\partial (V\Omega)}{\partial V}, \end{aligned} \tag{12}$$

where $\Omega = -\frac{1}{V\beta} ln\Xi$ is the thermodynamic potential density. It can be written in the functional form as $\Omega = f(T, \mu_i, m_i)$. If the masses of particles are independent of baryon number density $n_b = \left(\frac{N}{3V}\right)$ $(N = \sum N_i)$, one obtains $p = -\Omega$.

However, in the situation where the particle mass depends on the density or volume, one should have

$$p = -\Omega + n_b \frac{\partial \Omega}{\partial n_b}. \tag{13}$$

Now the statistical average for the energy is given by

$$\begin{aligned} \bar{E} &= \frac{1}{\Xi} \sum_{N_i,\alpha_c} E_{N_i,\alpha_c} e^{-\beta(E_{N_i,\alpha_c} - \sum_i \mu_i N_i)} \\ &= -\frac{\partial}{\partial \beta} ln\Xi + \sum_i \mu_i \bar{N}_i, \end{aligned} \tag{14}$$

where

$$\begin{aligned} \bar{N}_i &= \frac{1}{\Xi} \sum_{N_i,\alpha_c} N_i e^{-\beta(E_{N_i,\alpha_c} - \sum_i \mu_i N_i)} \\ &= \frac{1}{\beta} \left(\frac{\partial}{\partial \mu_i} ln\Xi \right)_{V,T,m_k} = -V \left(\frac{\partial \Omega}{\partial \mu_i} \right)_{T,m_k}, \end{aligned} \tag{15}$$

represents the average number of ith type particles. Hence, the energy density of such a system can be written as:

$$\begin{aligned} \rho &= \frac{\bar{E}}{V} = \frac{\partial(\beta\Omega)}{\partial \beta} + \sum_i \mu_i n_i \\ &= \Omega + \beta \frac{\partial \Omega}{\partial \beta} + \sum_i \mu_i n_i \\ &= \Omega + \sum_i \mu_i n_i - T \frac{\partial \Omega}{\partial T}. \end{aligned} \tag{16}$$

where n_i is the number density of particle type i and is given by

$$n_i = \frac{\bar{N}_i}{V} = -\left(\frac{\partial \Omega}{\partial \mu_i} \right)_{T,m_k} \tag{17}$$

The energy of the system in the MIT bag model in the microscopic regime is expressed as

$$E^{Bag}_{N_i,\alpha_c} = E_{N_i,\alpha_c} + BV. \tag{18}$$

The partition function becomes

$$\Xi^{Bag} = \sum_{N_i,\alpha_c} e^{-\beta(E_{N_i,\alpha_c} + BV - \sum_i \mu_i N_i)} = \Xi e^{-\beta BV}. \tag{19}$$

Therefore,

$$n_i^{Bag} = \frac{\bar{N}_i}{V} = -\left(\frac{\partial(\Omega + B)}{\partial \mu_i} \right)_{T,m_k,E_{N_i,\alpha_c},B}, \tag{20}$$

$$\begin{aligned} p^{Bag} &= \frac{1}{\beta} \frac{\partial ln\Xi^{Bag}}{\partial V} = \frac{1}{\beta} \frac{\partial (ln\Xi - \beta BV)}{\partial V} \\ &= -(\Omega + B) - V \frac{\partial(\Omega + B)}{\partial V}, \end{aligned} \tag{21}$$

$$\rho^{Bag} = \Omega + B + \sum_i \mu_i n_i - T \frac{\partial(\Omega + B)}{\partial T}. \tag{22}$$

Now, if we consider that the mass of the particle does not depend on the number density of baryon and the parameter B depends only on the energy density, then Eqs. (20)–(22) reduce to

$$n_i^{Bag} = -\left(\frac{\partial \Omega}{\partial \mu_i}\right), \tag{23}$$

$$p^{Bag} = -(\Omega + B) + n_b \frac{\partial B}{\partial n_b}, \tag{24}$$

$$\rho^{Bag} = \Omega + B + \sum_i \mu_i n_i, \tag{25}$$

In Eq. (24), the last term on the right hand side arises from the consideration that B depends on energy density. The additional term vanishes for constant B, and subsequently, the EoS of the interior matter reduces to that obtained in the MIT bag model.

5 EoS in the CFL phase

It is widely accepted that if the strange quark mass m_s is small enough, the CFL state would be the minimum energy configuration at high densities. In the case of the CFL phase of SQM, the constituent u, d and s quarks together form pairs and are compelled to take up equal Fermi momenta [32]. To obtain the EoS and relevant quantities, one must start with the thermodynamic potential density of the SQM in the context of the CFL phase. In the CFL phase of SQM at $T \to 0$, the thermodynamic potential density is given by [31,46,47].

$$\Omega = \frac{6}{\pi}\int_0^{\nu}(\kappa-\mu)\kappa^2 d\kappa - \frac{3}{\pi^2}\Delta_G^2\mu^2 + \frac{3}{\pi^2}\int_0^{\nu}[(\kappa^2+m_s^2)^{\frac{1}{2}} - \mu]\kappa^2 d\kappa, \tag{26}$$

where $\mu = \frac{\mu_u+\mu_d+\mu_s}{3}$, μ_u, μ_d and μ_s represent the chemical potentials of quarks u, d and s, respectively, and m_s is the strange quark mass. Δ_G represents the gap parameter in colour-superconductivity. In the CFL phase, the Fermi momentum of u, d and s quarks are the same [31,32]. This common Fermi momentum is determined by minimizing the free energy density up to order m_s^4 and is given by

$$\nu = 2\mu - \left(\mu^2 + \frac{m_s^2}{3}\right)^{\frac{1}{2}} = \mu - \frac{m_s^2}{6\mu} + \frac{m_s^4}{72\mu^3}. \tag{27}$$

Substituting Eq. (26) in Eqs. (20)–(22), we obtain the EoS in the CFL phase.

$$p = \frac{3\mu^4}{4\pi^2} - \frac{3m_s^2\mu^2}{4\pi^2} + \frac{1-12ln(\frac{m_s}{2\mu})}{32\pi^2}m_s^4 + \frac{3}{\pi^2}\Delta_G^2\mu^2 - B + n_b\frac{\partial B}{\partial n_b}, \tag{28}$$

$$\rho = \frac{9\mu^4}{4\pi^2} - \frac{3m_s^2\mu^2}{4\pi^2} + \frac{11m_s^4}{32\pi^2} + \frac{3ln(\frac{m_s}{2\mu})}{8\pi^2}m_s^4 + \frac{3}{\pi^2}\Delta_G^2\mu^2 + B, \tag{29}$$

$$n = \frac{\nu^3 + 2\Delta_G^2\mu}{\pi^2} = \frac{\mu^3}{\pi^2} - \frac{m_s^2\mu}{2\pi^2} + \frac{m_s^4}{8\pi^2\mu} + \frac{2\Delta_G^2\mu}{\pi^2}. \tag{30}$$

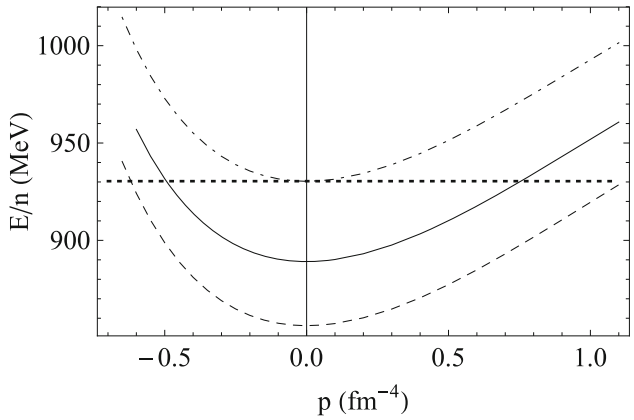

Fig. 2 Energy per baryon ($\frac{E}{n}$) vs pressure p of SQM in the CFL phase. Here dashed line is drawn for $m_s = 50$ MeV, solid line and dotdashed line represent $m_s = 150$ MeV and $m_s = 228.3$ MeV respectively. The energy per baryon for the horizontal line is 930.4 MeV which is the typical energy per baryon of ^{56}Fe. To draw the plots we have taken $\Delta_G = 100$ MeV

Zhu et al. [32] considered the density dependent B given in Eq. (10) predicted by Aguirre [45]. Using this density dependence of B, the energy associated with each baryon (E/n) is plotted as a function of pressure p and is shown in Fig. 2. In this model, zero pressure appears exactly at the lowest energy state. The minimum energy per baryon for $m_s = 228.3$ MeV touches the line for ^{56}Fe. Therefore, as per the stability of 3-flavor quarks is concerned, the upper limit of m_s is 228.3 MeV. The EoS in this model is visualized in Fig. 3. Here we have used the unit of ρ and p as fm^{-4}. The conversion is established as $1\,fm^{-1} = 197.3$ MeV [48].

6 Vaidya–Tikekar model EoS of different compact stars

In the standard procedure, to obtain the stellar structure of a compact star, one has to solve the TOV equation for a given EoS, using appropriate boundary conditions. However, in the Vaidya–Tikekar model, a geometry is given, and then one looks for a suitable composition of matter to support this geometry. The geometry is described by one free parameter λ known as the spheroidal parameter and another is known as the curvature parameter R to be determined. The EoS obtained from the V–T model assumes a linear form when the value of the parameter λ is large. In this geometrical model the stellar structures are found to be stable against small radial

oscillations. The EoS predicted by Gondek-Rosińska et al. [49] is in well agreement with the EoS predicted by Sharma et al. [50] for SAX J 1808.4-3658 from the V–T geometrical model. Thus it is interesting to note that the EoS obtained by considering geometry attached to the physical space of the compact object is consistent with that obtained from the microscopic composition of the interior matter of compact object, as both of them give a stable compact object having the same mass and radius. In the V–T model [38], a specific form of the g_{rr} metric component is prescribed, and using this metric ansatz, the general solution for the other metric component g_{tt} is obtained following the process prescribed by Mukherjee et al. [39]. The general solution is briefly outlined below.

We consider a static, spherically symmetric star whose interior metric is given by

$$ds^2 = -e^{2\gamma(r)}dt^2 + e^{2\xi(r)}dr^2 + r^2(d\theta^2 + sin^2\theta d\phi^2). \tag{31}$$

Considering the ansatz, predicted by Vaidya and Tikekar [38], given below

$$e^{2\xi} = \frac{1+\lambda\frac{r^2}{R^2}}{1-\frac{r^2}{R^2}}, \tag{32}$$

and assuming that inside the star matter distribution is similar to a perfect fluid with anisotropy in pressure, we have used the approach of Goswami et al. [41], which is the anisotropic extension of the solution obtained by Mukherjee et al. [39] and obtained the solution for the g_{tt} component of the metric function,

$$\psi(z) = e^{\gamma} = A\left[\frac{cos[(d+1)\zeta+\delta]}{d+1} - \frac{cos[(d-1)\zeta+\delta]}{d-1}\right], \tag{33}$$

where $\zeta = cos^{-1}z, z^2 = \frac{\lambda}{\lambda+1}(1-\frac{r^2}{R^2})$ and $d^2 = \lambda(1-\alpha)+2$. The energy-density ρ, radial (p_r) and transverse pressures (p_t) in this model are given by

$$\rho = \frac{1}{R^2(1-z^2)}\left[1+\frac{2}{(\lambda+1)(1-z^2)}\right], \tag{34}$$

$$p_r = -\frac{1}{R^2(1-z^2)}\left[1+\frac{2z}{(\lambda+1)}\left(\frac{\psi_z}{\psi}\right)\right], \tag{35}$$

$$p_t = p_r + \Delta, \tag{36}$$

where ψ_z represents the first derivative of function ψ with respect to variable z and $\Delta = \frac{\alpha\lambda[\lambda-(\lambda+1)z^2]}{R^2(\lambda+1)^2(1-z^2)^2}$ is the measure of the pressure anisotropy parametrized by α. The expression for the total mass contained within the radius b of a star is given below:

$$M(b) = \frac{(1+\lambda)\frac{b^3}{R^2}}{2(1+\lambda\frac{b^2}{R^2})}. \tag{37}$$

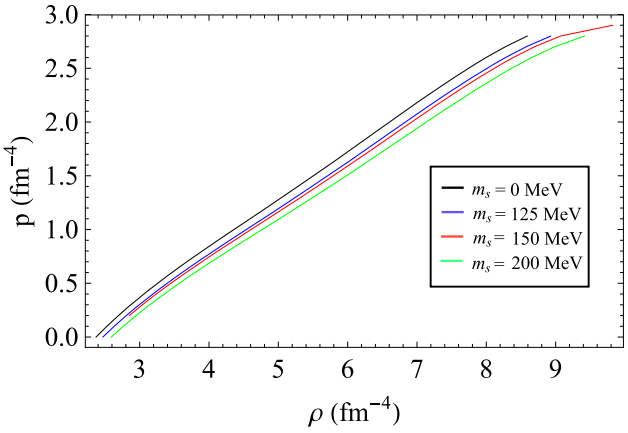

Fig. 3 Equation of state of SQM in the CFL phase with density dependent B

The model has four parameters, A, δ, R and λ, where λ is an input parameter and the rest will be fixed by imposing restrictions at the boundary of a star as given below.

1. At the boundary $(r = b)$ of a star, the interior metric should be finite and matched with the value obtained from the Schwarzschild exterior metric given below:

$$ds^2 = -\left(1-\frac{2M}{r}\right)dt^2 + \left(1-\frac{2M}{r}\right)^{-1}dr^2 + r^2\left(d\theta^2 + sin^2\theta d\phi^2\right). \tag{38}$$

Therefore, matching of the metric (31) and (38) at the boundary yields:

$$e^{2\xi} = \frac{1+\lambda\frac{b^2}{R^2}}{1-\frac{b^2}{R^2}} = \left(1-\frac{2M}{b}\right)^{-1}. \tag{39}$$

and

$$e^{2\gamma} = \left(1-\frac{2M}{b}\right). \tag{40}$$

2. Again at the surface of a star the radial pressure may be equated to zero which gives the following condition

$$\left(\frac{\psi_z}{\psi}\right)_{z_b} = -\frac{(\lambda+1)}{2z_b}. \tag{41}$$

Furthermore, taking the derivative of ψ into account in Eq. (33) with respect to z, we obtain the ratio $\left(\frac{\psi_z}{\psi}\right)$ at $z = z_b$ as

$$\left(\frac{\psi_z}{\psi}\right)_{z_b} = \frac{d^2-1}{\sqrt{1-z_b^2}}$$

$$\times\left[\frac{sin[(d+1)\zeta+\delta]-sin[(d-1)\zeta+\delta]}{(d-1)cos[(d+1)\zeta+\delta]-(d+1)cos[(d-1)\zeta+\delta]}\right]. \quad (42)$$

Thus, equating Eqs. (41) and (42), we can obtain the value of δ. As in this model, λ specifies the EoS of the interior matter of a star of given mass (M) and radius (b), and the choice of any one among radius (b), surface density (ρ_b) or central density (ρ_0) will determine the value of R for a given choice of λ. Thus, the present model accounts for a complete description of the physical properties of the star which includes the radial variation of energy density and radial pressure using Eqs. (34) and (35). The values of ρ and p_r are then used to determine the EoS of the interior matter.

7 Comparison of thermodynamic model with exactly solvable model

As we already have obtained the expressions for physical parameters such as energy density and pressures, we are now going to apply our model to some possible strange star candidates such as 4U 1820-30 [51], PSR J1614-2230 [52], PSR J1903+0327 [53], PSR J0030+0451 [54] and PSR J0740+6620 [55]. In the Vaidya–Tikekar model, the EoS of a star depends on both λ and α, therefore, by changing any of them, we can match the EoS of a given star with that obtained from thermodynamic point of view. In the present set up, we note that to fit the EoS of a star with the CFL EoS, the radius may be predicted. In Figs. 4, 5 and 6 we have plotted the EoS of the chosen compact objects and compared them with that of the CFL state. It is very interesting to note that our model permits a wide range of the model parameters λ and α for which strange quarks having CFL type EoS may be perceived inside compact objects. Another noteworthy feature is that to have a CFL type EoS, PSR J1614-2230 should be anisotropic in nature. In Table 1, we have tabulated the predicted radius and central density of compact objects as mentioned above by using (i) CFL EoS and (ii) MIT bag EoS. In the CFL phase, due to cooper pair formation, quarks collectively behave as bosons thereby overlooking the Pauli exclusion principle. This admits a more closed pack structure, and consequently, the central density of the star increases. Gravity, on the other hand, finds a new path to squeeze the star to a smaller size. This can be noted from Table 1.

8 Mass–radius relation of strange star admitting CFL EoS

We now study the mass–radius curve of compact objects by solving TOV equation comprised of strange matter having CFL type EoS. The mass–radius plot is shown in Fig. 7.

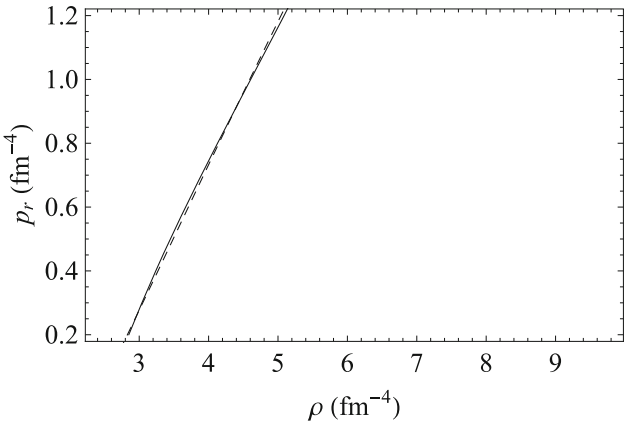

Fig. 4 Equation of state of SQM in the CFL phase with density dependent B (solid line) obtained from the thermodynamic model for $m_s = 150$ MeV and those obtained from VT model for the compact star 4U 1820-30 (dashed line) with predicted radius $b = 8.54\ km$. The model parameters are $\lambda = 5$ and $\alpha = 0$

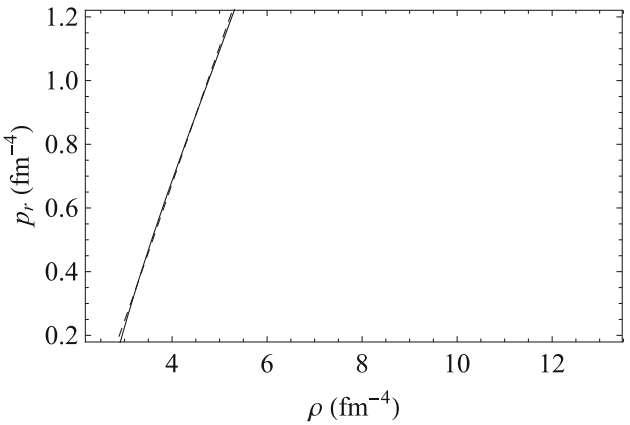

Fig. 5 Equation of state of SQM in the CFL phase with density dependent B (solid line) obtained from the thermodynamic model for $m_s = 200$ MeV and those obtained from VT model for the compact star PSR J1614-2230 (dashed line) with predicted radius $b = 8.46\ km$. The model parameters are $\lambda = 50$ and $\alpha = 0.39$

From the mass–radius plot, the maximum mass of strange star in the CFL EoS is found to be the maximum for $m_s = 0$ MeV, which is $\sim 3.61\ M_\odot$ and decreases when m_s increases. For instance, the maximum mass is $3.570\ M_\odot$ when $m_s = 100$ MeV, while it reduces to $3.458\ M_\odot$ when $m_s = 150$ MeV. These values of maximum masses are well above the value of $2.03\ M_\odot$ obtained by considering the MIT bag EoS for massless quarks ($m_s = 0$ MeV). Thus, we may conclude that the CFL EoS admits a wider range of compact objects, as indicated in the mass–radius plot in Fig. 7. The mass–central density plot reveals that the maximum density obtained from this model is 1.221×10^{15} g/cm^3 for $m_s = 0$ MeV, while for other values of m_s, it takes a lower value. It is to be noted that 1 MeV/fm^3 $= 1.78 \times 10^{12}$ g/cm^3 [56]. Above the maximum point, the mass (M) of a compact

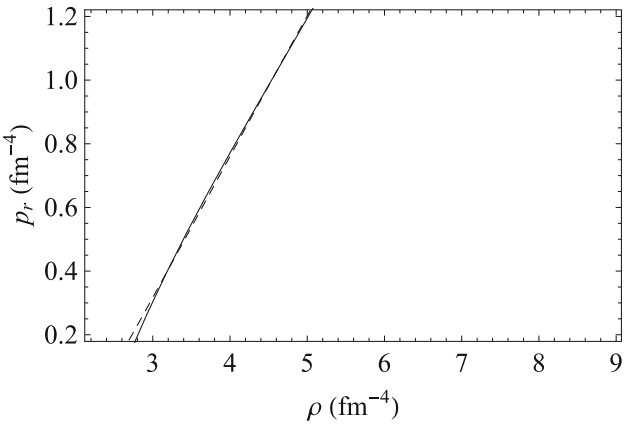

Fig. 6 Equation of state of SQM in the CFL phase with density dependent B (solid line) obtained from the thermodynamic model for $m_s = 125$ MeV and those obtained from VT model for the compact star PSR J1903+0327 (dashed line) with predicted radius $b = 8.5\ km$. The model parameters are $\lambda = 100$ and $\alpha = 0$

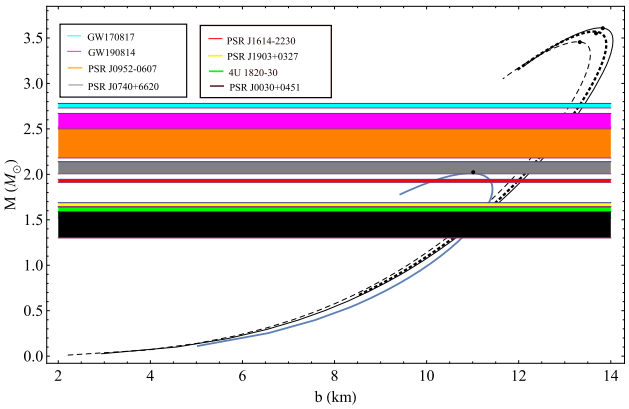

Fig. 7 Mass–radius plot of strange star composed of strange quark matter described by CFL EoS. Here solid, dotted and dashed line correspond to $m_s = 0$, 100 and 150 MeV respectively. Blue curve shows the mass radius relation for quark matter following the MIT bag EoS $p_r = \frac{1}{3}(\rho - 4B)$ with $B = 57.55$ MeV/fm^3. Mass ranges of different compact objects are also shown and indicated in the figure

object decreases with an increase in the value of central density (ρ_0), i.e., ($\frac{\partial M}{\partial \rho_0} < 0$), which corresponds to a collapsible state [57] and is not allowed as per stability is concerned. Interestingly, the maximum mass takes a higher value in the CFL phase than in the MIT bag model, as can be observed from Fig. 7. A physical justification can be made as follows: from Fig. 8 it is noted that the maximum central density of a star takes a lower value in the CFL phase than in the MIT bag model EoS. Therefore, as quarks form cooper pairs in the colour superconducting state, it takes away some part of the star's energy which is balanced by incorporating extra mass.

9 Energy conditions

For a relativistic sphere a physically realistic model is possible if the following energy conditions are satisfied at all the internal points and surface of the sphere [58,59].

1. Null Energy Condition (NEC): $\rho + p_r \geq 0$; $\rho + p_t \geq 0$.
2. Weak Energy Condition (WEC): $\rho + p_r \geq 0$; $\rho \geq 0$, $\rho + p_t \geq 0$.
3. Strong Energy Condition (SEC): $\rho + p_r \geq 0$; $\rho + p_r + 2p_t \geq 0$.
4. Dominant Energy Condition (DEC): $\rho \geq 0$; $\rho - p_r \geq 0$; $\rho - p_t \geq 0$.

In Figs. 9 and 10, we have plotted the Null Energy Conditions. In Figs. 9, 10 and 11, we have shown the Weak Energy Conditions. In Figs. 9 and 12, Strong Energy Conditions have been visualized. Figures 13 and 14 illustrate the Dominant Energy Conditions. From Figs. 9, 10, 11, 12, 13 and 14, we note that in this model, necessary energy conditions held good.

10 Herrera cracking condition

We know that a stellar model can be physically acceptable if both the square of the radial ($v_r^2 = \frac{dp_r}{d\rho}$) and transverse ($v_t^2 = \frac{dp_t}{d\rho}$) sound velocities remain below the velocity of light inside

Table 1 Tabulation of predicted radius and central density of some compact objects obtained from (i) CFL Eos and (ii) MIT bag Eos

Compact object	Mass ($M_\odot$)	λ	α	m_s (MeV)	Predicted radius (km)		Central density $\times 10^{15}$ (g/cm^3)	
					CFL EoS	MIT bag EoS	CFL Eos	MIT bag EoS
4U 1820-30 [51]	$1.58^{+0.06}_{-0.06}$	5	0	150	8.54	10.85	2.20	0.91
PSR J1614-2230 [52]	$1.928^{+0.017}_{-0.017}$	50	0.39	200	8.46	8.75	4.42	3.75
PSR J1903+0327 [53]	$1.667^{+0.021}_{-0.021}$	100	0	125	8.50	9.85	3.00	1.63
PSR J0030+0451 [54]	$1.44^{+0.15}_{-0.14}$	2.2	0	100	8.70	13	1.55	0.40
PSR J0740+6620 [55]	$2.072^{+0.067}_{-0.066}$	100	0.45	100	8.7	9.07	4.88	3.94

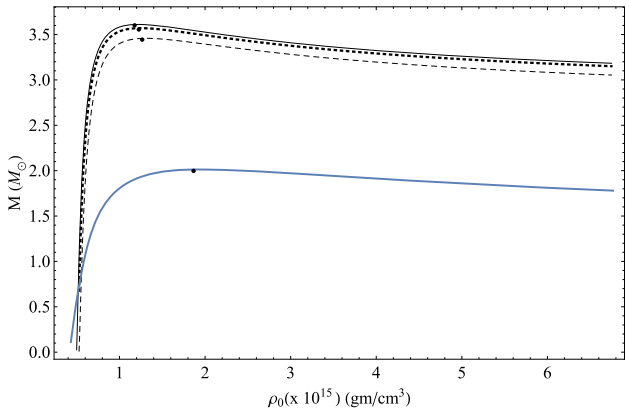

Fig. 8 Mass vs central density plot of strange star composed of strange quark matter described by CFL EoS. Here solid, dotted and dashed line correspond to $m_s = 0, 100$ and 150 MeV respectively. Blue curve shows the mass radius relation for quark matter following the MIT bag EoS $p_r = \frac{1}{3}(\rho - 4B)$ with $B = 57.55$ MeV/fm^3

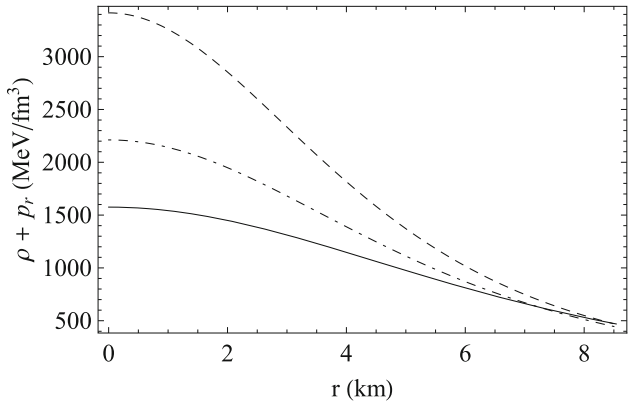

Fig. 9 Variation of $(\rho + p_r)$ with radial distance r for different compact objects. Here solid, dotdashed and dashed lines are drawn for 4U 1820-30, PSR J1903+0327 and PSR J1614-2230 respectively

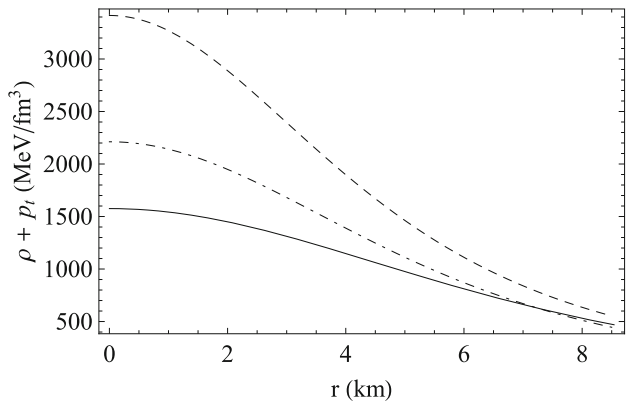

Fig. 10 Variation of $(\rho + p_t)$ with radial distance r for different compact objects. Here solid, dotdashed and dashed lines are drawn for 4U 1820-30, PSR J1903+0327 and PSR J1614-2230 respectively

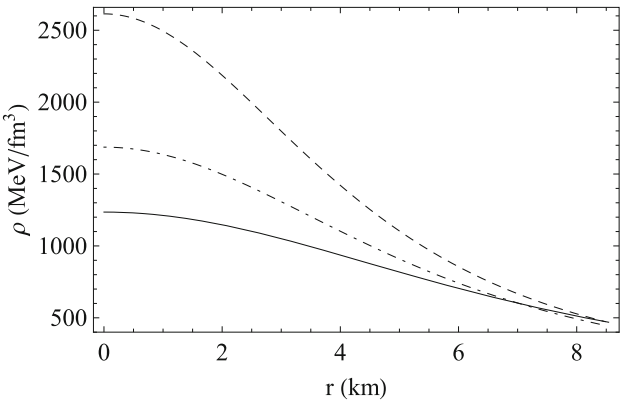

Fig. 11 Variation of ρ with radial distance r for different compact objects. Here solid, dotdashed and dashed lines are drawn for 4U 1820-30, PSR J1903+0327 and PSR J1614-2230 respectively

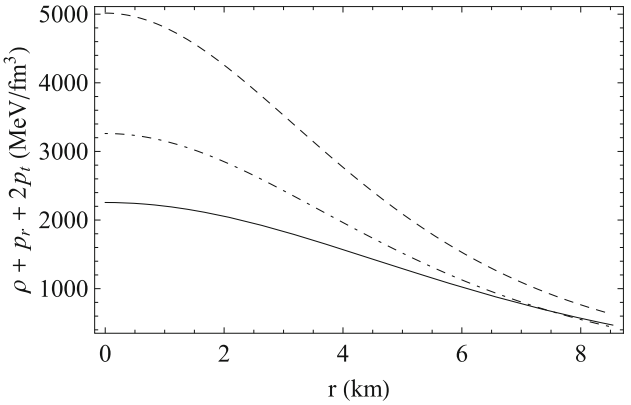

Fig. 12 Variation of $(\rho + p_r + 2p_t)$ with radial distance r for different compact objects. Here solid, dotdashed and dashed lines are drawn for 4U 1820-30, PSR J1903+0327 and PSR J1614-2230 respectively

a star, which is referred to as the 'causality condition'. In Figs. 15 and 16, we have plotted variations of v_r^2 and v_t^2 with r for different compact objects. It is found that the causality condition is obeyed in this model.

To check the stability of a stellar system, the concept 'cracking' was introduced by Herrera [60]. Based on this method, Abreu et al. [61] gave a criteria as given below:

$$0 \leq |v_t^2 - v_r^2| \leq 1. \tag{43}$$

It should be noted that for isotropic star $\frac{dp_r}{d\rho} = \frac{dp_t}{d\rho}$ and therefore for 4U 1608-52 and PSR J1903+0327, we must have $|v_t^2 - v_r^2| = 0$ at all interior points. Therefore, we have checked the validity of Abreu's inequality for PSR J1614-2230 only, which is shown in Fig. 17.

Again the condition $-1 \leq v_t^2 - v_r^2 \leq 1$ implies two distinct regions

$$-1 \leq (v_t^2 - v_r^2) \leq 0, \quad \text{potentially stable},$$
$$0 \leq (v_t^2 - v_r^2) \leq 1, \quad \text{potentially unstable}.$$

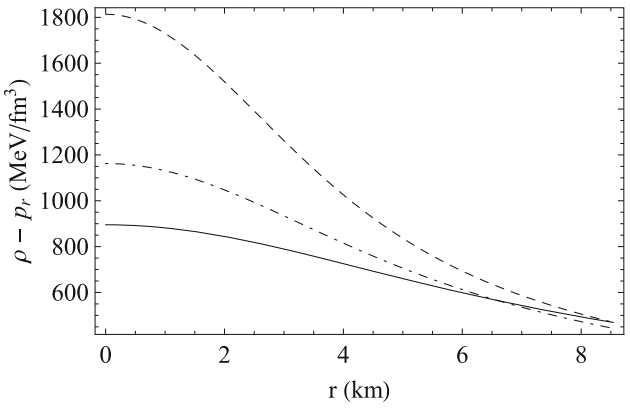

Fig. 13 Variation of $(\rho - p_r)$ with radial distance r for different compact objects. Here solid, dotdashed and dashed lines are drawn for 4U 1820-30, PSR J1903+0327 and PSR J1614-2230 respectively

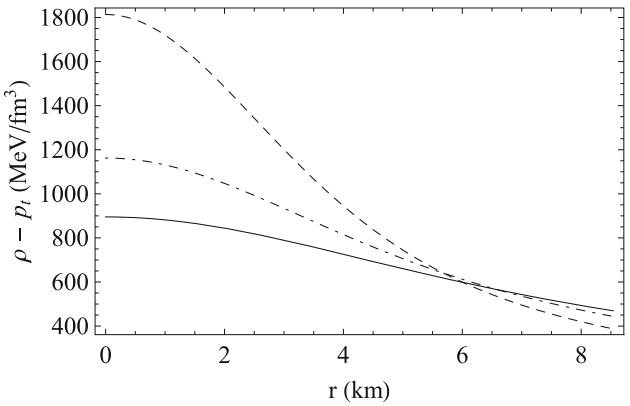

Fig. 14 Variation of $(\rho - p_t)$ with radial distance r for different compact objects. Here solid, dotdashed and dashed lines are drawn for 4U 1820-30, PSR J1903+0327 and PSR J1614-2230 respectively

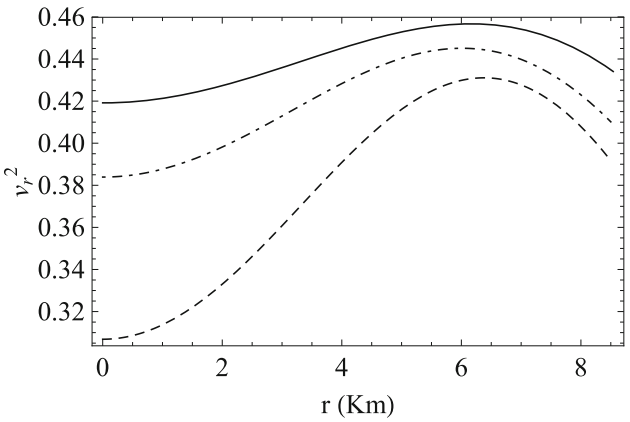

Fig. 15 Variation of v_r^2 with radial distance r inside various compact objects. Here solid, dotdashed and dashed lines are drawn for 4U 1820-30, PSR J1903+0327 and PSR J1614-2230 respectively

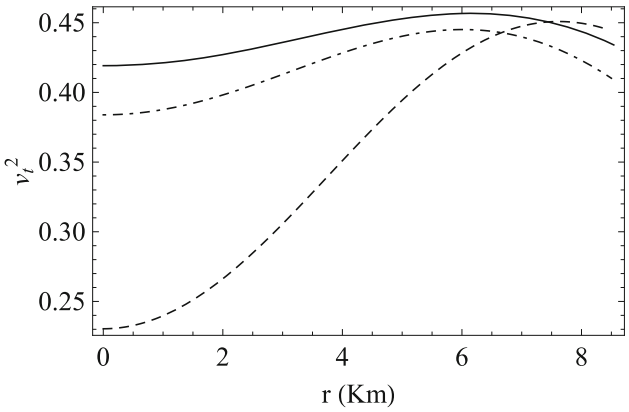

Fig. 16 Variation of v_t^2 with radial distance r inside various compact objects. Here solid, dotdashed and dashed lines are drawn for 4U 1820-30, PSR J1903+0327 and PSR J1614-2230 respectively

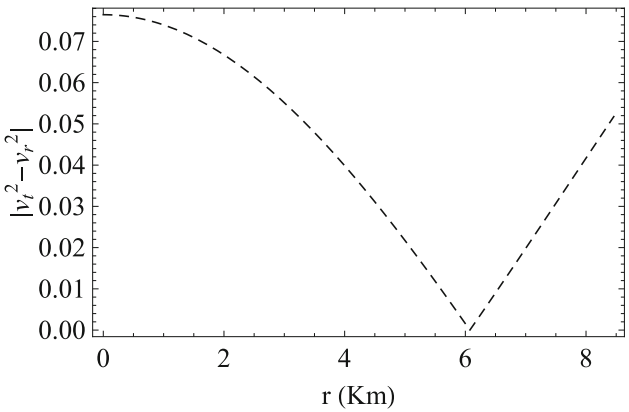

Fig. 17 Variation of $|v_t^2 - v_r^2|$ with radial distance r inside PSR J1614-2230

The plot in Fig. 18 indicates that there is region inside the star where $(v_t^2 - v_r^2)$ alters sign and therefore changes from a potentially stable to a potentially unstable region.

Moreover, the difference between each sound speed should follow the physical restriction $|v_t^2 - v_r^2| \leq 1$, as the individual sound speed must be less than the speed of light. This is crucial in view of the characterization of a particular model to investigate whether the model is potentially unstable. For a set of nonphysical fluctuations in energy density and anisotropy, it can be possible to check the cracking points within a given configuration, i.e., $|v_t^2 - v_r^2| > 1$, but the existence of such cracking points could not point out the physical stellar models that are potentially unstable.

11 Adiabatic index

The adiabatic index (Γ) is an important thermodynamic quantity describing any instability inside a compact object. For adiabatic perturbations, the entropy remains constant, for

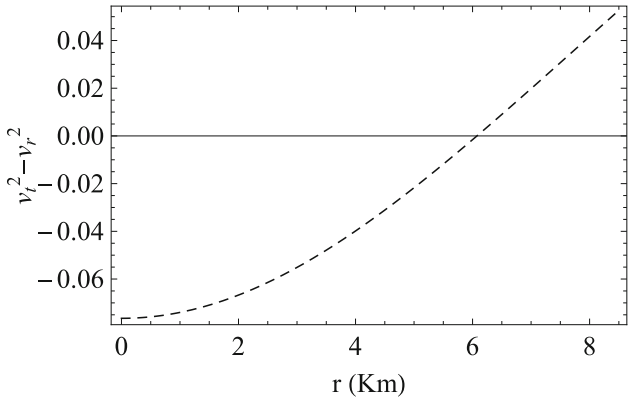

Fig. 18 Variation of $(v_t^2 - v_r^2)$ is shown against radial distance r inside PSR J1614-2230

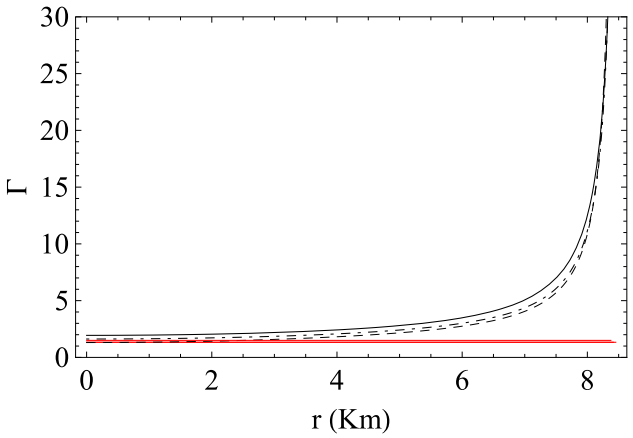

Fig. 19 Variation of adiabatic index (Γ) against radial distance r inside various compact objects. Here solid, dotdashed and dashed lines are drawn for 4U 1820-30, PSR J1903+0327 and PSR J1614-2230 respectively. Horizontal red line corresponds to the value Γ'

such an instability, the adiabatic index can be expressed in the form [62]

$$\Gamma = \frac{\rho + p_r}{p_r}\frac{dp_r}{d\rho}. \tag{44}$$

For the stability of a Newtonian fluid sphere, the adiabatic index must be greater than $\frac{4}{3}$ [63]. However, Chan et al. modified this limit for a relativistic anisotropic fluid sphere and showed that for stability $\Gamma > \Gamma'$. Where

$$\Gamma' = \frac{4}{3} - \left[\frac{4}{3}\frac{(p_r - p_t)}{|p_r'|r}\right]_{max}. \tag{45}$$

For our model we have found that the value of Γ is always larger than the limit Γ' as evident from Fig. 19.

12 Conclusions

In this paper, we have obtained a class of solutions for relativistic compact objects in spheroidal geometry with a matter distribution that is anisotropic in nature and obeys the colour-flavor-locked (CFL) equation of state. The metric ansatz in spheroidal geometry was introduced by Vaidya and Tikekar [38], in which the t = constant hypersurface has the geometry of a three-spheroid embedded in a four dimensional Euclidean space and stipulates a law of variation of density determined by the curvature of the physical 3-space. Assuming a density dependence of the B-parameter according to Aguirre [45], the energy per baryon in the CFL phase is evaluated, which seems to take a minimum value at zero external pressure, as evident from Fig. 2. The minima of the plots increase with increasing mass of the strange quark (m_s) and touch the line corresponding to the energy per baryon of ^{56}Fe ($\sim$ 930.4 MeV) for $m_s = 228.3$ MeV. Thus, 3-flavor quark matter (SQM) in the CFL phase is absolutely stable relative to ^{56}Fe for $m_s < 228.3$ MeV. The stability of SQM increases with a decrease in the value of m_s. For example, when $m_s = 150$ MeV, the energy per baryon is approximately 889.2 MeV, which represents weakly bound SQM compared to the value 856.1 MeV when $m_s = 50$ MeV. To apply the EoS, obtained from thermodynamics to some observed compact objects, we have considered the compact objects 4U 1820-30, PSR J1614-2230, PSR J1903+0327, PSR J0030+0451 and PSR J0740+6620. It has been found that a wider range of λ is allowed for which CFL EoS may be obtained inside these compact objects. Apart from that, PSR J1614-2230 and PSR J0740+6620 are found to be anisotropic in nature with values of anisotropy parameter $\alpha = 0.39$ and 0.45, respectively, while others show isotropic pressure distribution. In our article, we have shown that the CFL equation of state from thermodynamic point of view may be described from a geometrical point of view considering the Vaidya–Tikekar metric ansatz with a proper choice of metric parameter λ and anisotropy parameter α. Using the choice of such parameters, we have predicted the radius of the above mentioned recently observed compact objects. The radius prediction of such pulsars considering the CFL EoS and MIT bag EoS suggest that the CFL EoS gives relatively smaller radii compared to the MIT bag EoS, which can be noted from Table 1. In the CFL phase, quarks form cooper pairs that collectively behave as bosons, hence, by virtue, they do not need to obey Pauli's exclusion principle. Thus, gravity can shrink the star to a more compact structure, and as a result, its radius decreases. As our approach theoretically predicts the maximum mass of Strange Quark Star as high as 3.61 $M_\odot$, a wide range of observed masses, which includes pulsars and secondary objects of GW170817 and GW190814 events, may be predicted. From the mass–radius plots in Fig. 7, it is noted that the CFL EoS puts a limit on the maximum mass, which is $\sim$ 3.61 $M_\odot$ when $m_s = 0$ MeV, $\Delta_G = 100$ MeV, and decreases further for higher values of m_s. This is because the CFL EoS becomes softer for higher values of m_s, as evident from Fig. 3. The same argument is also valid for MIT bag EoS. A com-

parison is made with the MIT bag EoS, which shows that the CFL EoS allows a higher value of maximum mass than the MIT bag EoS for which $M_{max} = 2.03\ M_\odot$. Such a high value of maximum mass permits our model to include a wider range of compact objects, which is also indicated in Fig. 7. In comparison with the maximum mass obtained by Jasim et al. [12] for CFL EoS and constant B, our model predicts a much higher value of maximum mass for the same values of m_s and Δ_G in the presence of density dependent B. Therefore, it may be concluded that a large value of stellar mass ($> 2M_\odot$) may be accommodated with density dependent B and CFL EoS in our proposed model. In particular, the theory with CFL EoS and nonzero strange quark mass ($m_s \neq 0$) can achieve the 3.61 $M_\odot$ which is a value hardly attainable in general relativity even if we consider fast rotation effects too. After the discovery of GW190814 event, the mass of the secondary object is found to be $2.59^{+0.08}_{-0.09}\ M_\odot$ [64]. The recently measured mass of PSR J0952-0607 is found to be $2.35 \pm 0.17\ M_\odot$ [65], the heaviest and fastest pulsar detected so far in the disk of the Milky Way, supporting the possible presence of strange quark matter in its composition. Such observed high mass may be accommodated in our present model with nonzero m_s. From Fig. 8, it is evident that the maximum central density permitted by the CFL EoS is 1.221 $\times\ 10^{15}$ g/cm^3. Above the maximum mass point it is noted that $\frac{\partial M}{\partial \rho_0} < 0$, which is not allowed since this leads to instability of a fluid sphere [57]. From Figs. 9, 10, 11, 12, 13 and 14, it is obvious that all the necessary energy conditions are obeyed in this model. The causality conditions and the inequality given by Abreu et al. [61] are satisfied, as shown in Figs. 15, 16, 17 and 18. For stability against small adiabatic perturbations, we calculate the value of the adiabatic index Γ from Eq. (44) and study its radial variation, which is plotted in Fig. 19. It is evident that at all interior points, the value of Γ is greater than Γ' according to Eq. (45), thus showing that our model is stable against small perturbations for adiabatic flow.

Acknowledgements KBG is thankful for the fellowship provided by CSIR vide no. 09/1219(0004)/2019-EMR-I.

Funding A fellowship has been provided to K.B. Goswami by Council of Scientific and Industrial Research, India (vide no. 09/1219(0004)/2019-EMR-I).

Data Availability Statement This manuscript has no associated data or the data will not be deposited. [Author's comment: We have used only observed mass and radius of some known compact objects to construct relativistic stellar models].

Declarations

Conflict of interest Not applicable.

Funded by SCOAP^3. SCOAP^3 supports the goals of the International Year of Basic Sciences for Sustainable Development.

References

1. E. Witten, Phys. Rev. D **30**, 272 (1984)
2. A. Chodos, R.L. Jaffe, K. Johnson, C.B. Thorne, V.F. Weisskopf, Phys. Rev. D **9**, 3471 (1974)
3. E. Farhi, R.L. Jaffe, Phys. Rev. D **30**, 2379 (1984)
4. M. Brilenkov, M. Eingorn, L. Jenkovszky, A. Zhuk, JCAP **08**, 002 (2013)
5. L. Paulucci, J.E. Horvath, Phys. Lett. B **733**, 164 (2014)
6. J.D.V. Arbañil, M. Malheiro, JCAP **11**, 012 (2016)
7. G. Lugones, J.D.V. Arbañil, Phys. Rev. D **95**, 064022 (2017)
8. S.R. Chowdhury, D. Deb, S. Ray, F. Rahaman, B.K. Guha, Int. J. Mod. Phys. D **29**, 2050001 (2020)
9. P. Haensel, J.L. Zdunik, R. Schaeffer, Astron. Astrophys. **160**, 121 (1986)
10. C. Alcock, E. Farhi, O. Olinto, Astrophys. J. **310**, 261 (1986)
11. T. Tangphati, G. Panotopoulos, A. Banerjee, A. Pradhan, Chin. J. Phys. **82**, 62 (2023)
12. M.K. Jasim, A. Pradhan, A. Banerjee, T. Tangphati, G. Panotopoulos, Mod. Phys. Lett. A **36**, 2150227 (2021)
13. Ksh.N. Singh, A. Banerjee, S.K. Maurya, F. Rahaman, A. Pradhan, Phys. Dark Universe **31**, 100774 (2021)
14. T. Tangphati, S. Hansraj, A. Banerjee, A. Pradhan, Phys. Dark Universe **35**, 100990 (2022)
15. T. Tangphati, A. Pradhan, A. Banerjee, G. Panotopoulos, Phys. Dark Universe **33**, 100877 (2021)
16. G. Lugones, J.E. Horvath, Astron. Astrophys. **403**, 173 (2003)
17. D.D. Ivanenko, D.F. Kurdgelaidze, Lett. Nuovo Cim. **IIS1**, 13 (1969)
18. D.D. Ivanenko, D.F. Kurdgelaidze, Sov. Phys. J. **13**, 1015 (1970)
19. B.C. Barrois, Nucl. Phys. B **129**, 390 (1977)
20. B.C. Barrois, *Non-perturbative effects in dense quark matter*, Ph.D. thesis, California Institute of Technology, Pasadena, California, UMI 79-04847 (1979)
21. S.C. Frautschi, Presented at Workshop on Hadronic Matter at Extreme Energy Density, Erice (1978)
22. R.S. Bogadi, M. Govender, S. Moyo, Phys. Rev. D **102**, 043026 (2020)
23. S. Thirukkanesh, A. Kaisavelu, M. Govender, Eur. Phys. J. C **80**, 214 (2020)
24. P. Mafa Takisa, S.D. Maharaj, M.L. Lekala, Astrophys. Space Sci. **366**, 102 (2021)
25. H. Reinhardt, B.V. Dang, Phys. Lett. B **173**, 473 (1986)
26. S. Chakrabarty, S. Raha, B. Sinha, Phys. Lett. B **229**, 112 (1989)
27. S. Chakrabarty, Phys. Rev. D **43**, 627 (1991)
28. S. Chakrabarty, Phys. Rev. D **48**, 1409 (1993)
29. S. Chakrabarty, Phys. Rev. D **54**, 1306 (1996)
30. G.X. Peng, H.C. Chiang, B.S. Zou, P.J. Ning, S.J. Luo, Phys. Rev. C **62**, 025801 (2000)
31. N. Prasad, R. Bhalerao, Phys. Rev. D **69**, 1003001 (2004)

32. M.F. Zhu, G.Z. Liu, Z. Yu, Y. Zu, W.T. Song, Sci. China Ser. G **52**(10), 1506 (2009)
33. L. Herrera, N.O. Santos, Phys. Rep. **286**, 53 (1997)
34. R. Kippenhahn, A. Weigert, *Steller Structure and Evolution* (Springer, Berlin, 1990)
35. R.A. Broglia, V. Zelevinsky (eds.), *Fifty Years of Nuclear BCS: Pairing in Finite Systems* (World Scientific Publishing Co. Pte. Ltd., Singapore, 2013)
36. R.F. Sawyer, Phys. Rev. Lett. **29**, 382 (1972)
37. A.I. Sokolov, J. Exp. Theor. Phys. **79**, 1137 (1980)
38. P.C. Vaidya, R. Tikekar, J. Astrophys. Astron. **3**, 325 (1982)
39. S. Mukherjee, B.C. Paul, N.K. Dadhich, Class. Quantum Gravity **14**, 3475 (1997)
40. R. Sharma, S. Das, M. Govender, D.M. Pandya, Ann. Phys. **414**, 168079 (2020)
41. K.B. Goswami, A. Saha, P.K. Chattopadhyay, Class. Quantum Gravity **39**, 175006 (2022)
42. B. Muller, J. Rafelski, Phys. Lett. B **101**, 111 (1981)
43. Y.-X. Liu, D.-F. Gao, H. Guo, Nucl. Phys. A **695**, 353 (2001)
44. G.F. Burgio, M. Baldo, P.K. Sahu, A.B. Santra, H.J. Schulze, Phys. Lett. B **526**, 19 (2002)
45. R. Aguirre, Phys. Lett. B **559**, 207 (2003)
46. M. Alford, S. Reddy, Phys. Rev. D **67**, 074024 (2003)
47. M. Alford, K. Rajagopal, S. Reddy, Phys. Rev. D **64**, 074017 (2001)
48. M. Guidry, *Gauge Field Theories, An Introduction with Applications* (WILEY-VCH Verlag GmbH & Co. KGaA, Weinheim, 2004), p.512
49. D. Gondek-Rosińska, T. Bulik, L. Zdunik, E. Gourgoulhon, S. Ray, J. Dey, M. Dey, Astron. Astrophys. **363**, 1005 (2000)
50. R. Sharma, S. Mukherjee, M. Dey, J. Dey, Mod. Phys. Lett. A **17**, 827 (2002)
51. T. Güver, P. Wroblewski, L. Camarota, F. Özel, Astrophys. J. **719**, 1807 (2010)
52. M.C. Miller, Astrophys. J. **822**, 27 (2016)
53. P.C.C. Freire et al., Mon. Not. R. Astron. Soc. **412**, 2763 (2011)
54. M.C. Miller et al., ApJL **887**, L24 (2019)
55. T.E. Riley et al., ApJL **918**, L27 (2021)
56. T. Miyatsu, S. Yamamuro, K. Nakazato, arXiv:1308.6121v1 [astro-ph.HE]
57. Y.B. Zeldovich, I.D. Novikov, *Relativistic Astrophysics, Stars and Relativity*, vol. 1 (University of Chicago Press, Chicago, 1971)
58. B.P. Brassel, S.D. Maharaj, R. Goswami, Prog. Theor. Exp. Phys. **2021**, 103E01 (2021)
59. B.P. Brassel, S.D. Maharaj, R. Goswami, Entropy **23**, 1400 (2021)
60. L. Herrera, Phys. Lett. A **165**, 206 (1992)
61. H. Abreu, H. Hernández, L.A. Núñez, Class. Quantum Gravity **24**, 4631 (2007)
62. M. Merafina, R. Ruffini, Astron. Astrophys. **221**, 4 (1989)
63. H. Heintzmann, W. Hillebrandt, Astron. Astrophys. **38**, 51 (1975)
64. R. Abbott et al., ApJL **896**, L44 (2020)
65. G.A. Carvalho et al., Eur. Phys. J. C **82**, 1096 (2022)